

# Effect of Primordial Black Holes on the global 21-cm signal

Atrideb Chatterjee<sup>1,\*</sup>

Kapteyn Astronomical Institute, University of Groningen, PO Box 800, 9700 AV Groningen, The Netherlands

January 16, 2026

## ABSTRACT

The 21-cm global signal, a treasure trove of information about the nature of the first luminous sources of the Universe, has traditionally been modelled assuming that these early sources were predominantly star-forming galaxies. However, recent observations by the James Webb Space Telescope (JWST) have revealed several AGNs as early as  $z \sim 10 - 10.4$ . In light of this, it is important to investigate the contribution of such AGNs to the 21-cm signal. Assuming that these AGNs are seeded by Primordial Black Holes (PBHs) and employing an analytical PBH model, consistent with existing cosmological and astrophysical constraints, we show that these exotic objects can have a significant impact on the redshift evolution of the global signal.

**Key words.** galaxies: high-redshift / quasars: general / cosmology: theory / dark ages / reionization / first stars

## 1. Introduction

The sky-averaged 21-cm signal, also known as the global 21-cm signal, originates from the hyperfine transition of neutral hydrogen in the intergalactic medium (IGM). The redshift evolution of this signal carries information about the thermal and ionization state of the IGM, which in turn is governed by the nature, timing, and intensity of the first astrophysical sources (e.g. Pritchard & Loeb 2012; Greig & Mesinger 2015; Kern et al. 2017; Greig & Mesinger 2018; Gillet et al. 2019; Mesinger 2019; Ghara et al. 2021; Chatterjee et al. 2021; Hutter et al. 2021; Trebitsch et al. 2023a). As a result, the global 21-cm signal contains a wealth of information about the properties of these early sources. Most of the existing galaxy formation models assume these early sources to be of star-forming natures, with active galactic nuclei (AGN) contributing significantly only at later times ( $z \sim 5$ ) (Onoue et al. 2017; Dayal et al. 2020; Trebitsch et al. 2023b; Dayal et al. 2025).

Very recently, James Webb Space Telescope (JWST) observations have revealed that some of these early sources at  $z \sim 10 - 10.4$  are in fact AGNs rather than the star-forming galaxies (Bogdán et al. 2024; Kovács et al. 2024; Napolitano et al. 2024). Given that some of the properties of these AGNs (such as the elevated black hole-to-stellar mass ratios) are difficult to reconcile within the standard galaxy formation models (Matteri et al. 2025; Zhang et al. 2025; Nelander et al. 2025; Dayal & maiolino 2025), one of the alternative pathways to explain them are the primordial black holes (PBHs) (Dayal 2024; Dayal & maiolino 2025; Matteri et al. 2025; Nelander et al. 2025; Zhang et al. 2025). If a fraction of PBHs, originated at the time of inflation (Hawking 1971; Carr & Hawking 1974; Carr 2005; Carr & Kühn 2020), indeed seeded early galaxies, their accelerated formation and growth could significantly influence the thermal and ionization state of the IGM at very early epoch of the Universe, when galaxy formation would not have been sufficiently underway — an effect not accounted for in most of the 21-cm signal forecasts

carries out so far (e.g., Barkana & Loeb 2001; Furlanetto et al. 2006; Chatterjee et al. 2023; Dhandha et al. 2025; Sims et al. 2025; Gessey-Jones et al. 2025). Although, a number of studies (Tashiro & Sugiyama 2013; Ewall-Wice et al. 2020; Yang 2021; Mittal et al. 2022; Nelander et al. 2025, e.g.,) indeed took into account AGNs while modelling the 21-cm signal, their aim was to explain the non-standard feature of the 21-cm signal tentatively detected by the EDGES experiment (Bowman et al. 2018), which has later been ruled out at a 95.3% confidence level by the Shaped Antenna Measurement of the Background Radio Spectrum 3 (SARAS-3) experiment (Singh et al. 2022).

In this work, we investigate the imprints of PBH-seeded galaxies on the global 21-cm signal. We start with a simple semi-analytical model for star-forming (SF) galaxies, consistent with recent observations of the high-redshift Universe, and add the contribution of the PBH-seeded systems to determine the impact of these exotic objects on the 21-cm signal. While similar in spirit to Nelander et al. (2025), our model employs a more fundamental model for the PBH-seeded systems based on Dayal & maiolino (2025). Furthermore, the PBH model is consistent with the existing cosmological and astrophysical constraints.

This question is timely, given ongoing and planned experiments targeting the global 21-cm signal, including SARAS-3 (Singh et al. 2022), the Large-Aperture Experiment to Detect the Dark Ages (LEDA; Greenhill & Bernardi 2012), SCI-HI (Voytek et al. 2014), the Broadband Instrument for Global Hydrogen Reionisation Signal (BIGHORNS; Sokolowski et al. 2015), the Radio Experiment for the Analysis of Cosmic Hydrogen (REACH; Cummer et al. 2022), and the Cosmic Twilight Polarimeter (CTP; Nhan et al. 2018).

Throughout this paper, we adopt a  $\Lambda$ CDM model with dark energy, dark matter and baryonic densities in units of the critical density as  $\Omega_\Lambda = 0.685$ ,  $\Omega_m = 0.315$  and  $\Omega_b = 0.049$ , respectively, a Hubble constant  $H_0 = 100h \text{ km s}^{-1} \text{ Mpc}^{-1}$  with  $h = 0.67$ , spectral index  $n_s = 0.96$  and normalisation  $\sigma_8 = 0.81$  (Planck Collaboration et al. 2020).

The paper is organised as follows. In Sec. 2, we describe the theoretical model of the SF galaxies and the PBH-seeded

\* e-mail: a.chatterjee@rug.nl

systems. While Sec. 3 presents the modelling of the 21 cm signal, Sec. 4 describes the effect of PBHs on the 21-cm signal. We summarise our results and conclusions in Sec. 5.

## 2. Theoretical Model

Our theoretical framework comprises two distinct components: the first accounts for early SF galaxies, whereas the second component models a population of PBHs that assemble their host galaxies around themselves.

### 2.1. The semi-analytic model for star-forming galaxies

As this work aims to determine the effect of PBH-seeded galaxies on the global 21-cm signal, any standard model of star-forming galaxies, as long as it does not violate any existing observational constraints of the high-z Universe (i.e., reionisation and UV Luminosity Function), the model will be sufficient for this work. Keeping this in mind, we take a very simple model for star-forming galaxies at  $z \gtrsim 6$ , as described below.

1. In this model, the Star Formation Rate Density (SFRD) at a redshift  $z$  is given by

$$\rho_{\text{SFR}} = \frac{1}{t_{\text{dyn}}(z)} \frac{\Omega_b}{\Omega_m} \int_{M_{\min}(z)} dM_h \frac{dn}{dM_h} f_{\star}(M_h) M_h \quad (1)$$

with  $M_h$  being the mass of the halo,  $t_{\text{dyn}}(z)$  being the dynamical time scale at redshift  $z$ , and  $\frac{dn}{dM_h}$  is the halo mass function given by Tinker et al. (2008) implemented using the publicly available python package `colossus` (Diemer 2018). The factor,  $t_{\text{dyn}}(z)$  arising in the denominator of the right-hand side of the equation as we assume the star formation in haloes to be spread over the entire  $t_{\text{dyn}}(z)$  following Chiu & Ostriker (2000). Finally,  $M_{\min}(z)$  is the minimum mass of halos allowed for star formation. Under the simplified assumption of atomic cooling to be the only channel responsible for cooling, we determine  $M_{\min}(z)$  corresponding to a virial temperature of  $10^4$  K (Barkana & Loeb 2001)<sup>1</sup>. Following Donnan et al. (2024), we take the star formation efficiency to be

$$f_{\star}(M_h) = \frac{2f_0}{(M_h/M_p)^{-\beta} + (M_h/M_p)^{\gamma}} \quad (2)$$

with  $\{f_0, M_p, \beta, \gamma\} = \{0.16, 10^{11.7}, 0.9, 0.65\}$ . This choice of the star formation efficiency ensures that the UV Luminosity Function (UFLF) predicted from this model is consistent with the measurement from the high redshift JWST observations (Donnan et al. 2024). We also note that this functional form is not physically motivated but is rather obtained from a data-driven point of view.

2. The number of photons produced per unit time at frequency  $\nu$  at a redshift  $z$  is computed using

$$\dot{n}_{\nu} = \frac{dN_{\nu}}{dM} \times \rho_{\text{SFR}} \quad (3)$$

where  $\frac{dN_{\nu}}{dM}$  is the number of photons produced at frequency  $\nu$  per unit stellar mass. We calculate this from Starburst99 (Leitherer et al. 1999) assuming a standard Salpeter IMF in the mass range  $1 - 100 M_{\odot}$  with a metallicity of  $0.05 M_{\odot}$ .

3. The number of ionising photons produced intrinsically inside galaxies at a redshift  $z$  is computed as

$$\dot{n}_{\text{ion}}(z) = \int_{\nu_H}^{\infty} \dot{n}_{\nu}(z) d\nu \quad (4)$$

where  $\nu_H$  is the threshold frequency for hydrogen photoionisation.

4. The number of ionizing photons coming out of a galaxy that can reionize the IGM is given by  $\dot{n}_{\text{ion,esc}}^{\text{SF}} = f_{\text{esc}} \dot{n}_{\text{ion}}^{\text{int}}$ , we fix the value of ionizing escape fraction  $f_{\text{esc}} = 0.2$  making sure that the model matches with the existing reionization constraints as shown in the Appendix-A.
5. The effect of the astrophysically produced, i.e., “normal” AGN, is ignored in this model. This is justified by the fact that the effect of these “normal” AGN starts to dominate around  $z \sim 5$  (Dayal et al. 2025), whereas our redshift range of interest lies at a higher redshift, i.e.,  $z \sim 30 - 6$ .

### 2.2. The formation and evolution of PBH-seeded galaxies

In modelling the PBH-seeded galaxy population, we closely follow the analytic framework proposed by Dayal & maiolino (2025) except for the change in the mass function of the PBH-seeded galaxies. We also rigorously check that the model, even after changing the mass function, is still consistent with the existing cosmological and astrophysical constraints. Here, we briefly outline the salient (and relevant for 21-cm signal) features and the changes we made to this model

1. In Dayal & maiolino (2025), the authors use the simplified power law mass function, whereas in this work, we assume the more popular log-normal function, as this is a reasonable approximation for a range of PBH mechanisms (Clesse & García-Bellido 2015; Blinnikov et al. 2016). Following Carr (1975), we take

$$\frac{dN}{dM_{\text{PBH}}} = \frac{\kappa}{M_{\text{PBH}}^2 \sqrt{2\pi\sigma^2}} \exp\left[-\frac{1}{2} \left(\frac{\ln(M_{\text{PBH}}/M_c)}{\sigma}\right)^2\right] \quad (5)$$

with  $\kappa$  being the normalizing constant,  $M_c$  being the characteristic mass of PBHs, and  $\sigma$  is the standard deviation of the distribution. The value of  $\kappa$  is determined by matching with the value of the observed mass function of  $10^{-5.27} \text{ cMpc}^{-3}$  at  $z \sim 10$  (Kovács et al. 2024; Bogdán et al. 2024) assuming an average seed mass value of  $10^{3.65} M_{\odot}$ . Further, we assume  $\sigma = 0.7$  (Matteri et al. 2025) and take the characteristic mass,  $M_c$ , to be equal to the average seed mass i.e.,  $M_c = 10^{3.65} M_{\odot}$ .

2. The bolometric luminosity of a PBH-seeded galaxy is calculated from

$$L_{\text{bol}} = \frac{\epsilon_r M_{\text{BH}}^{\text{ac}} c^2}{\Delta t} L_{\odot} \quad (6)$$

where  $c$  is the speed of light,  $L_{\odot}$  is the solar luminosity,  $\epsilon_r$  is the radiative efficiency and  $M_{\text{BH}}^{\text{ac}}$  is the accreted BH mass within one time step  $\Delta t$ . While  $\epsilon_r$  is taken as 0.057 (Dayal & maiolino 2025), the accreted BH mass  $M_{\text{BH}}^{\text{ac}}$  is calculated assuming an Eddington fraction  $f_{\text{edd}} = 0.25$  following the procedure described in detail in Dayal (2024).

3. We calculate the photon production rate at a frequency  $\nu$  at redshift  $z$  from a PBH-seeded galaxy with

$$\dot{n}_{\nu}^{\text{PBH}} = \int_{L_{\text{B},\min}}^{\infty} dM_{\text{PBH}} \frac{dN}{dM_{\text{PBH}}} \frac{L_{\nu}(M_{\text{PBH}})}{h_p \nu} \quad (7)$$

<sup>1</sup> We would like to point out that this simplified assumption is a reasonable approximation for the high redshift range we are working in (Barkana & Loeb 2001; Furlanetto et al. 2006)

where  $L_\nu$  is the luminosity of individual galaxies at frequency  $\nu$ . For each galaxy, we first compute the B-band luminosity  $L_B$  from bolometric luminosity using the fitting formula from Marconi et al. (2004) and then assume a spectral index of  $-0.57$  ( $-1.57$ ) to compute Ly- $\alpha$  (Ionising) photon production rate from  $L_B$ .

4. The escape fraction of the ionizing photons is given by  $f_{\text{esc}}^{\text{PBH}} = \exp(-\tau_{\text{PBH}})$ , where  $\tau_{\text{PBH}}$  is the dust optical depth determined by the metal enrichment and the Eddington fraction of the PBH-seeded galaxy as described in detail in Dayal & maiolino (2025) and Dayal et al. (2025). Therefore, the total number of ionising photons escaping into the IGM is given by  $\dot{n}_{\text{ion,esc}}^{\text{PBH}} = f_{\text{esc}}^{\text{PBH}} \dot{n}_{\text{ion,int}}^{\text{PBH}}$ , with  $\dot{n}_{\text{ion,int}}^{\text{PBH}}$  being the total number of ionising photons produced inside the PBH-seeded system.
5. The X-ray luminosity is calculated from the bolometric luminosity ( $L_{\text{bol}}$ ) with the fitting functions provided in Duras et al. (2020).

### 3. The 21-cm global signal

The sky-averaged 21-cm brightness temperature can be written as (Chatterjee et al. 2020)

$$T_b(\nu) = 10.1 \text{ mK } x_{\text{HI}}(z) \left( 1 - \frac{T_\gamma(z)}{T_S(z)} \right) (1+z)^{1/2} \quad (8)$$

where  $x_{\text{HI}}(z)$  is the neutral Hydrogen fraction of the IGM at redshift  $z$ ,  $T_\gamma(z)$  is the background CMB temperature given by  $T_\gamma = 2.73(1+z)$  K. Further,  $T_S$ , the spin temperature of the Hydrogen atom, can be written as

$$T_S^{-1} = \frac{T_\gamma^{-1} + x_\alpha T_K^{-1} + x_c T_K^{-1}}{1 + x_c + x_\alpha} \quad (9)$$

where  $x_\alpha$  is the Ly- $\alpha$  coupling coefficients,  $x_c$  is the collisional coupling coefficient and  $T_K$  is the kinetic temperature of the IGM. While the collisional coupling coefficient,  $x_c$  is determined using the standard formalism and the fitting functions provided in Pritchard & Loeb (2012), we describe all the other terms in more detail below.

#### 3.1. Kinetic temperature of the IGM

The two main processes that determine the redshift evolution of the IGM kinetic temperature ( $T_K$ ) are adiabatic cooling due to the expansion of the Universe and the X-ray heating of the IGM.

While the adiabatic cooling has been computed trivially following Furlanetto et al. (2006), computation of X-ray heating is highly uncertain given our poor knowledge of the high-redshift Universe. Assuming that the relation between X-ray luminosity and the star formation rate density (SFRD) in the high- $z$  Universe follows from the local Universe, we compute the X-ray emissivity using Mineo et al. (2012)

$$\frac{\epsilon_X^{\text{SF}}}{\text{J sec}^{-1} \text{Mpc}^3} = 3.4 \times 10^{33} \frac{\rho_{\text{SFR}}}{\text{M}_\odot \text{yr}^{-1} \text{Mpc}^3} \quad (10)$$

where  $\rho_{\text{SFR}}$  is the star formation rate density obtained from the star-forming galaxies as described in Eqn 1.

The X-ray emissivity coming from PBH-seeded galaxies is given by

$$\epsilon_X^{\text{PBH}}(z) = \int_{M_{\text{min, PBH}}}^{M_{\text{max, PBH}}} \frac{dn}{dM_{\text{PBH}}} \cdot L_X^{\text{PBH}}(M_{\text{PBH}}) dM_{\text{PBH}} \quad (11)$$

The total X-ray coming out of the SF and PBH seeded galaxies (i.e., SF+PBH) and heating the IGM is given by

$$\epsilon_X^{\text{SF+PBH}}(z) = f_h [f_{X,\text{esc}}^{\text{SF}} \epsilon_X^{\text{SF}}(z) + f_{X,\text{esc}}^{\text{PBH}} \epsilon_X^{\text{PBH}}(z)] \quad (12)$$

where  $f_h$  is the fraction of the total X-ray that will heat the IGM and is fixed to 0.2 (Furlanetto et al. 2006). Moreover,  $f_{X,\text{esc}}^{\text{SF}}$  and  $f_{X,\text{esc}}^{\text{PBH}}$  are the escape fractions of X-ray from SF and PBH galaxies, respectively. We also note that uncertainties in the  $\epsilon_X - \rho_{\text{SFR}}$  relationship, i.e., eqn-12, that may arise from the poorly constrained nature of SF galaxies at high redshift can be effectively absorbed into the parameter  $f_{X,\text{esc}}^{\text{SF}}$  (as it will come as a multiplicative factor). In this work,  $f_{X,\text{esc}}^{\text{SF}}$  is kept fixed at 1 and  $f_{X,\text{esc}}^{\text{PBH}}$  is varied in the range 0.1–1.0. We have discussed the effect of varying  $f_{X,\text{esc}}^{\text{PBH}}$  in detail in Section 4.

#### 3.2. Ly- $\alpha$ coupling

The Ly- $\alpha$  coupling coefficient  $x_\alpha$  is written as

$$x_\alpha = 1.81 \times 10^{11} (1+z)^{-1} S_\alpha \frac{J_\alpha}{\text{cm}^{-2} \text{sec}^{-1} \text{Hz}^{-1} \text{sr}^{-1}} \quad (13)$$

Here  $S_\alpha$  is taken to be order unity (Furlanetto et al. 2006) coming from a detailed analysis of atomic physics.

Finally, the background Ly- $\alpha$  flux  $J_\alpha$  in the presence of both SF and PBH-seeded galaxies is given by

$$J_\alpha^{\text{SF+PBH}} = \frac{c}{4\pi} (1+z)^3 \int_z^{z_{\text{max}}} \left[ f_\alpha^{\text{SF}} \dot{n}_{\nu'}^{\text{SF}}(z') + f_\alpha^{\text{PBH}} \dot{n}_{\nu'}^{\text{PBH}}(z') \right] \left| \frac{dt'}{dz'} \right| dz' \quad (14)$$

where  $\dot{n}_{\nu'}^{\text{SF}}(z)$  is the photon production rate at a frequency  $\nu'$  at a redshift  $z$  from SF galaxies and  $\dot{n}_{\nu'}^{\text{PBH}}$  is the contribution from the PBHs as mentioned before. Further  $f_\alpha^{\text{SF}}$  and  $f_\alpha^{\text{PBH}}$  are the escaping fraction of the Ly- $\alpha$  photons from SF and PBH-seeded galaxies. For the sake of simplicity, we assume both of them to be 1. Finally, the integration upper limit,  $z_{\text{max}}$ , is calculated using (Chatterjee et al. 2020)

$$1 + z_{\text{max}} = \frac{\nu_H}{\nu_\alpha} (1+z) \quad (15)$$

with  $\nu_\alpha$  denoting the Ly- $\alpha$  frequency. The upper frequency cutoff ensures that continuum ionising photons — those that would be absorbed by the neutral IGM — are excluded, since they do not contribute to the production of Ly- $\alpha$  photons in the background.

#### 3.3. Reionization

The neutral Hydrogen fraction,  $x_{\text{HI}}$ , determined from the evolution of the volume filling factor for ionised Hydrogen ( $Q_{\text{HII}}$ ), in the presence of PBH galaxies along with the SF galaxies, can be written as

$$\frac{dQ_{\text{HII}}}{dt} = \frac{\dot{n}_{\text{ion,esc}}^{\text{PBH}} + \dot{n}_{\text{ion,esc}}^{\text{SF}}}{n_{\text{H,com}}} + Q_{\text{HII}} \alpha_B C n_{\text{H,com}} (1+z)^3 \quad (16)$$

where  $n_{\text{H,com}}$  is the hydrogen comoving number density,  $C$  is the clumping factor of the IGM and  $\alpha_B$  is the (case B) recombination rate coefficient. The functional form of clumping factor  $C$  is taken as  $1 + 43z^{-1.71}$  (Pawlik et al. 2009). Finally,  $\dot{n}_{\text{ion,esc}}^{\text{SF}}$  and  $\dot{n}_{\text{ion,esc}}^{\text{PBH}}$  denote the rate of ionising photons escaping out to IGM from SF and PBHs, respectively.

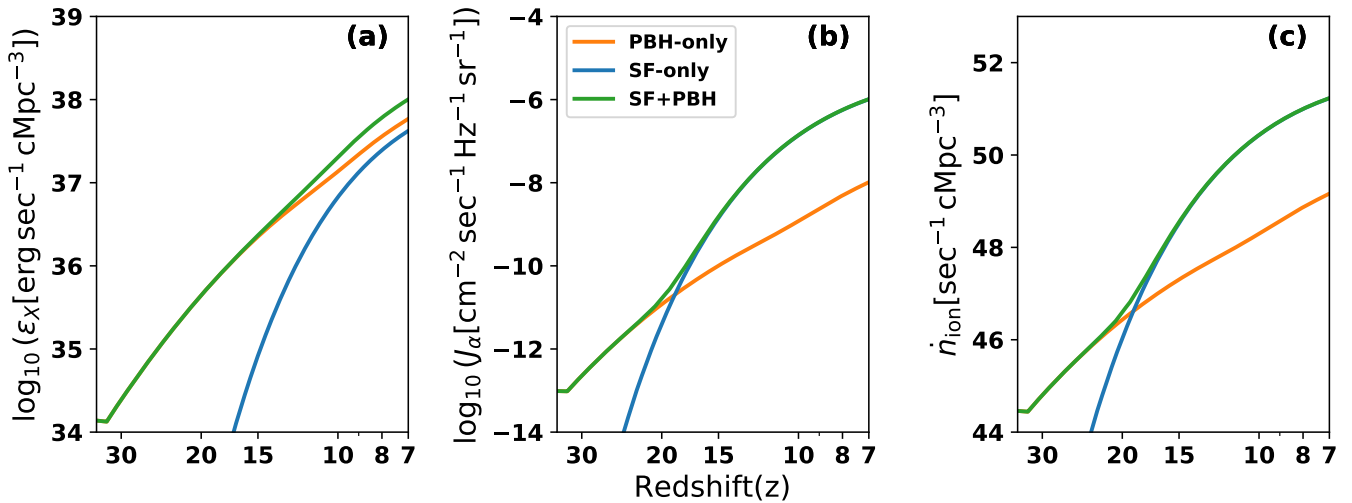


**Fig. 1.** Redshift evolution of key quantities that affect the 21-cm signal. The orange, blue, and green curves correspond to contributions from **PBH-only**, **SF-only**, and **SF+PBH** galaxies, respectively. **Panel (a):** Intrinsic X-ray emissivity as a function of redshift. In this case, **PBH-only** dominates over **SF-only** across the entire redshift range. **Panel (b):** Evolution of the Ly- $\alpha$  background flux. While dominated by PBH-seeded sources for the very early redshift around  $z = 30 - 20$ , the **SF-only** completely dominates the redshift  $z = 20 - 7$ . **Panel (c):** Ionizing photon emissivity, which mimics the Ly- $\alpha$  background trends.

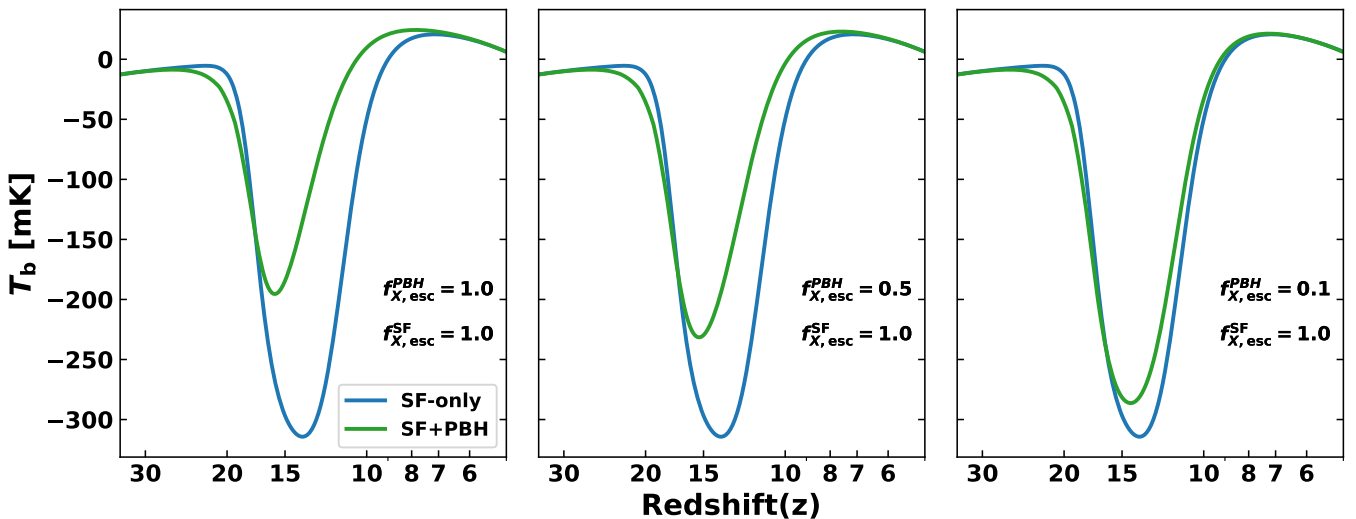


**Fig. 2.** Redshift evolution of the global 21-cm signal for different values of  $f_{X,\text{esc}}^{\text{PBH}}$ , as indicated in the plots. The blue and green curves correspond to the **SF-only** and **SF+PBH** scenarios, respectively. In the leftmost panel, with  $f_{X,\text{esc}}^{\text{PBH}} = 1$ , the **SF-only** case exhibits a much deeper absorption trough compared to the **SF+PBH** scenario. This difference arises because the additional X-ray emission from PBH-seeded galaxies heats the intergalactic medium (IGM) more efficiently, thereby reducing the depth of the absorption feature. As  $f_{X,\text{esc}}^{\text{PBH}}$  decreases (moving towards the right), the X-ray output from PBH-seeded galaxies diminishes, leading to a progressively smaller difference between the two signals. We also note the difference in the signals around  $25 \gtrsim z \gtrsim 20$ , and this can be attributed to the fact that **SF+PBH** produces significantly more Ly- $\alpha$  photons compared to **SF-only** model, as is also evident in Panel (b) of 1.

#### 4. Effect of PBHs on 21-cm signal

We begin by describing the redshift evolution of key quantities shown in panels (a)–(c) of Fig. 1. The orange, blue, and green curves correspond to contributions from **PBH-only**, **SF-only**, and **SF+PBH** galaxies, respectively.

In panel (a), we find the intrinsic X-ray emissivity at early redshifts ( $z \sim 34 - 15$ ) to be dominated by PBH-seeded galaxies, with negligible contribution from SF galaxies. It is only around  $z \sim 10$  that the SF galaxy's contribution starts becoming non-negligible. This is expected, as the black holes

in PBH-seeded AGNs accrete surrounding gas and produce copious amounts of X-ray photons much before the onset of SF galaxies, and therefore significantly outshine the emission from SF galaxies across the whole redshift range.

Panels (b) and (c) show the Ly- $\alpha$  flux and ionising photon production rate. They are dominated by PBH-seeded systems in the very early redshift range  $30 \gtrsim z \gtrsim 20$ , the epoch when the SF galaxies are yet to form. However, once star-forming galaxies begin to emerge, they rapidly surpass the PBH-seeded systems in photon production around  $z \sim 20$ , indicating that stars are the primary sources of these photons.

To summarise, the X-ray photon budget is dominated by PBH-seeded galaxies across all redshifts, whereas the Ly- $\alpha$  and ionising photon contributions are dominated by PBHs only at very early times ( $30 \gtrsim z \gtrsim 20$ ); at later times ( $z \lesssim 20$ ), SF galaxies become the primary sources of Ly- $\alpha$  and ionising photons.

Next, we move to Fig. 2 which shows the global 21-cm signal for the **SF-only** and **SF+PBH** models over the redshift range  $34 \gtrsim z \lesssim 5$ . In all the panels, the escape fraction of X-rays from SF galaxies,  $f_{X,esc}^{SF}$ , is fixed at 1, while the escape fraction from PBH-seeded galaxies,  $f_{X,esc}^{PBH}$ , decreases from 1.0 to 0.1 from left to right.

In the leftmost panel, where  $f_{X,esc}^{PBH} = 1.0$  i.e., same as that of the SF galaxies, the **SF+PBH** model produces a noticeably shallower absorption trough, with an amplitude of  $\sim -200$  mK at  $z \sim 18$ , compared to the **SF-only** model, which shows a deeper trough of amplitude  $\sim -300$  mK at  $z \sim 16$ . This difference arises because, in the **SF+PBH** case, the X-ray contribution from PBH-seeded galaxies, dominating across all the redshifts (as also shown in Fig. 1), enhances the heating of the IGM at these redshifts.

As we go to the next panel on the right, with  $f_{X,esc}^{PBH} = 0.5$ , i.e., X-ray escape fraction of PBHs is half of that of the SF-galaxies, we see that the difference between these two signals starts to decrease. Finally, at the rightmost panel, with  $f_{X,esc}^{PBH}$  as one-tenth of that of the SF-galaxies, the amplitude of the absorption trough of **SF-only** and **SF+PBH** becomes very similar.

We also note that the signal coming from **SF+PBH** in the redshift range  $z = 25 - 20$ , near the first inflection point, is slightly different from **SF-only** in all the panels. This is attributed to the fact that the **SF+PBH** produces more Ly- $\alpha$  photons than that of the **SF-only**, as also shown in Panel (b) of Fig. 1. We further note that this difference in signal remains the same in all the panels as the Ly- $\alpha$  escape fraction is kept fixed for both models, i.e.,  $f_{\alpha}^{SF} = f_{\alpha}^{PBH} = 1$  across all the panels, confirming that this difference originates due to Ly- $\alpha$  production and therefore independent of the X-ray emission in the models.

Next, we focus on the redshift range  $10 \gtrsim z \gtrsim 7$ . As is well known, the 21 cm signal in this regime is primarily determined by the neutral hydrogen fraction of the IGM. Considering that the **SF-only** model are already consistent with existing reionization constraints (as shown in the Appendix-A), and that the contribution of PBHs<sup>2</sup> to the ionizing photon budget is negligible (as shown in panel (c) of Fig. 1), all models predict a similar neutral hydrogen fraction within this redshift range. Consequently, the resulting 21 cm signals from all models show similar behaviour.

## 5. Conclusions and Discussion

In this work, we investigate the effects of including the PBH-seeded galaxies, in addition to the star-forming galaxies, on the global 21-cm signal. Our main findings are

- Assuming that the escape fraction of X-ray photons from PBH-seeded galaxies same as that of SF galaxies, i.e.  $f_{X,esc}^{PBH} = f_{X,esc}^{SF}$ , the 21-cm signal is strongly affected by the enhanced X-ray heating produced by these systems. This additional heating makes the absorption trough of the 21-cm signal significantly shallower compared to the **SF-only** scenario.

<sup>2</sup> Contribution of the Astrophysical Black Holes are shown to be negligible in Dayal et al. (2025)

As we decrease the value of  $f_{X,esc}^{PBH}$  from 1.0 to 0.1, the difference between these signals diminishes.

- The number of the Ly- $\alpha$  photons coming from the PBH-seeded galaxies is dominating the Ly- $\alpha$  photon budget in the redshift range  $z = 30 - 20$  compared to those produced from star-forming galaxies; they alter the signal in this redshift regime  $25 \gtrsim z \gtrsim 20$ .
- Finally, the number of ionising photons coming from the PBH-seeded galaxies is 2-3 orders of magnitude lower compared to those produced from star-forming galaxies in the redshift range  $z = 10 - 7$ . Therefore, the introduction of PBHs leaves the reionisation constraints unaffected.

We will end by highlighting some of the shortcomings of this work. First of all, we did not include the radio emission that may come from these PBH-seeded systems. Secondly, there is no rigorous justification for choosing the lognormal mass function for the PBH-seeded systems. We are planning to investigate the effect of different mass functions of PBHs on the 21-cm signal in future work. Thirdly, we vary the X-ray escape fraction for the PBHs, but did not vary the Ly- $\alpha$  photon escape fraction; in principle, one should vary both these parameters simultaneously. In future, we are also planning to address the effect of simultaneously varying different free parameters that appear in PBH-seeded galaxies using an MCMC framework.

*Acknowledgements.* The work of AC was supported by the European Union’s Horizon Europe research and innovation programme under the Marie Skłodowska-Curie Postdoctoral Fellowship HORIZON-MSCA-2023-PF-01, grant agreement No 101151693 (LUPCOS). AC gratefully acknowledges Pratika Dayal, Tirthankar Roy Choudhury, Koushiki, and Amrita Banerjee for their constructive feedback on the manuscript. AC acknowledges the use of CHATGPT for refining the text at the final stage of the manuscript.

## References

Barkana, R. & Loeb, A. 2001, Phys. Rep., 349, 125  
 Blinnikov, S., Dolgov, A., Porayko, N. K., & Postnov, K. 2016, J. Cosmology Astropart. Phys., 2016, 036  
 Bogdán, Á., Goulding, A. D., Natarajan, P., et al. 2024, Nature Astronomy, 8, 126  
 Bowman, J. D., Rogers, A. E. E., Monsalve, R. A., Mozdzen, T. J., & Mahesh, N. 2018, Nature, 555, 67  
 Carr, B. & Kühn, F. 2020, Annual Review of Nuclear and Particle Science, 70, 355  
 Carr, B. J. 1975, ApJ, 201, 1  
 Carr, B. J. 2005, arXiv e-prints, astro  
 Carr, B. J. & Hawking, S. W. 1974, MNRAS, 168, 399  
 Chatterjee, A., Choudhury, T. R., & Mitra, S. 2021, MNRAS, 507, 2405  
 Chatterjee, A., Dayal, P., Choudhury, T. R., & Schneider, R. 2020, MNRAS, 496, 1445  
 Chatterjee, A., Dayal, P., & Mauerhofer, V. 2023, MNRAS, 525, 620  
 Chiu, W. A. & Ostriker, J. P. 2000, ApJ, 534, 507  
 Chornock, R., Berger, E., Fox, D. B., et al. 2013, ApJ, 774, 26  
 Clesse, S. & García-Bellido, J. 2015, Phys. Rev. D, 92, 023524  
 Cumner, J., de Lera Acedo, E., de Villiers, D. I. L., et al. 2022, Journal of Astronomical Instrumentation, 11, 2250001  
 Davies, F. B., Hennawi, J. F., Bañados, E., et al. 2018, ApJ, 864, 142  
 Dayal, P. 2024, A&A, 690, A182  
 Dayal, P. & maiolino, R. 2025, arXiv e-prints, arXiv:2506.08116  
 Dayal, P., Volonteri, M., Choudhury, T. R., et al. 2020, MNRAS, 495, 3065  
 Dayal, P., Volonteri, M., Greene, J. E., et al. 2025, A&A, 697, A211  
 Dhandha, J., Fialkov, A., Gessey-Jones, T., et al. 2025, MNRAS, 542, 2292  
 Diemer, B. 2018, ApJS, 239, 35  
 Donnan, C. T., McLure, R. J., Dunlop, J. S., et al. 2024, MNRAS, 533, 3222  
 Duras, F., Bongiorno, A., Ricci, F., et al. 2020, A&A, 636, A73  
 Ewall-Wice, A., Chang, T.-C., & Lazio, T. J. W. 2020, MNRAS, 492, 6086  
 Furlanetto, S. R., Oh, S. P., & Briggs, F. H. 2006, Phys. Rep., 433, 181  
 Gessey-Jones, T., Sartorio, N. S., Bevins, H. T. J., et al. 2025, Nature Astronomy, 9, 1268  
 Ghara, R., Giri, S. K., Ciardi, B., Mellema, G., & Zaroubi, S. 2021, MNRAS, 503, 4551

Gillet, N., Mesinger, A., Greig, B., Liu, A., & Ucci, G. 2019, MNRAS, 484, 282

Greenhill, L. J. & Bernardi, G. 2012, arXiv e-prints, arXiv:1201.1700

Greig, B. & Mesinger, A. 2015, MNRAS, 449, 4246

Greig, B. & Mesinger, A. 2018, MNRAS, 477, 3217

Greig, B., Mesinger, A., & Bañados, E. 2019, MNRAS, 484, 5094

Hawking, S. 1971, MNRAS, 152, 75

Hutter, A., Dayal, P., Yepes, G., et al. 2021, MNRAS, 503, 3698

Jin, X., Yang, J., Fan, X., et al. 2023, ApJ, 942, 59

Kern, N. S., Liu, A., Parsons, A. R., Mesinger, A., & Greig, B. 2017, ApJ, 848, 23

Kovács, O. E., Bogdán, Á., Natarajan, P., et al. 2024, ApJ, 965, L21

Leitherer, C., Schaerer, D., Goldader, J. D., et al. 1999, ApJS, 123, 3

Marconi, A., Risaliti, G., Gilli, R., et al. 2004, MNRAS, 351, 169

Mason, C. A., Treu, T., Dijkstra, M., et al. 2018, ApJ, 856, 2

Matteri, A., Pallottini, A., & Ferrara, A. 2025, A&A, 697, A65

McGreer, I. D., Mesinger, A., & D'Odorico, V. 2015, MNRAS, 447, 499

Mesinger, A., ed. 2019, The Cosmic 21-cm Revolution, 2514-3433 (IOP Publishing)

Mineo, S., Gilfanov, M., & Sunyaev, R. 2012, MNRAS, 419, 2095

Mittal, S., Ray, A., Kulkarni, G., & Dasgupta, B. 2022, J. Cosmology Astropart. Phys., 2022, 030

Napolitano, L., Castellano, M., Pentericci, L., et al. 2024, arXiv e-prints, arXiv:2410.18763

Nelander, A., Cain, C., DSilva, J. C. J., et al. 2025, arXiv e-prints, arXiv:2507.21230

Nhan, B. D., Bordenave, D. D., Bradley, R. F., et al. 2018, arXiv e-prints, arXiv:1811.04917

Onoue, M., Kashikawa, N., Willott, C. J., et al. 2017, ApJ, 847, L15

Pawlak, A. H., Schaye, J., & van Scherpenzeel, E. 2009, MNRAS, 394, 1812

Planck Collaboration, Aghanim, N., et al. 2020, A&A, 641, A5

Pritchard, J. R. & Loeb, A. 2012, Reports on Progress in Physics, 75, 086901

Schenker, M. A., Ellis, R. S., Konidaris, N. P., & Stark, D. P. 2014, ApJ, 795, 20

Schroeder, J., Mesinger, A., & Haiman, Z. 2013, MNRAS, 428, 3058

Sims, P. H., Bevins, H. T. J., Fialkov, A., et al. 2025, MNRAS[arXiv:2504.09725]

Singh, S., Jishnu, N. T., Subrahmanyam, R., et al. 2022, Nature Astronomy, 6, 607

Sokolowski, M., Tremblay, S. E., Wayth, R. B., et al. 2015, PASA, 32, e004

Tashiro, H. & Sugiyama, N. 2013, MNRAS, 435, 3001

Tinker, J., Kravtsov, A. V., Klypin, A., et al. 2008, ApJ, 688, 709

Totani, T., Kawai, N., Kosugi, G., et al. 2006, PASJ, 58, 485

Trebitsch, M., Hutter, A., Dayal, P., et al. 2023a, MNRAS, 518, 3576

Trebitsch, M., Hutter, A., Dayal, P., et al. 2023b, MNRAS, 518, 3576

Ďurovčíková, D., Katz, H., Bosman, S. E. I., et al. 2020, MNRAS, 493, 4256

Voytek, T. C., Natarajan, A., Jáuregui García, J. M., Peterson, J. B., & López-Cruz, O. 2014, ApJ, 782, L9

Yang, Y. 2021, Phys. Rev. D, 104, 063528

Zhang, S., Liu, B., Bromm, V., et al. 2025, ApJ, 987, 185

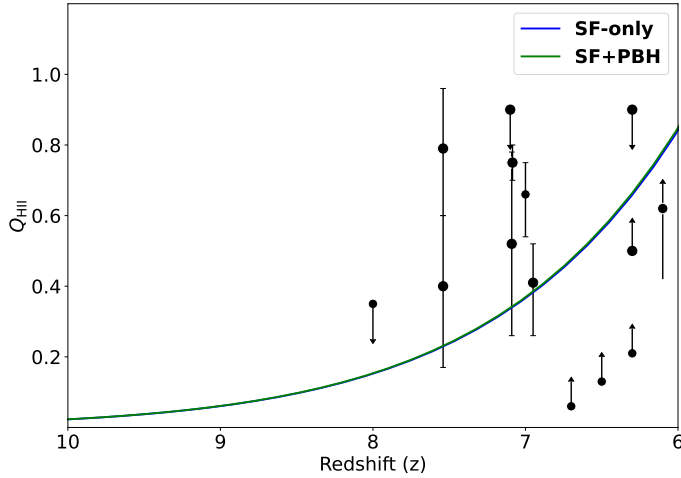


**Fig. A.1.** The redshift evolution of the volume filling factor of HII region,  $Q_{\text{HII}}$ . The data points are collected from different observations as mentioned in the text.

### Appendix A: Redshift evolution of $Q_{\text{HII}}$ for different models

Here we show the redshift evolution of the volume filling factor of HII region,  $Q_{\text{HII}}$ , coming from **SF-Only** and **SF+PBH** and how they compare with the existing observations related to reionisation. From Fig A.1, it is evident that the evolution of  $Q_{\text{HII}}$  coming from **SF-Only** and **SF+PBH** are practically identical, and they match quite well with the existing observational data points (Totani et al. 2006; Chornock et al. 2013; Schroeder et al. 2013; Schenker et al. 2014; McGreer et al. 2015; Davies et al. 2018; Mason et al. 2018; Greig et al. 2019; Ďurovčíková et al. 2020; Jin et al. 2023). The fact overlap between  $Q_{\text{HII}}$  from **SF-Only** and **SF+PBH** arises because the PBH contribution to the ionizing photon budget is negligible, as discussed in the main text.